Cement and Concrete Research 146 (2021) 106491

Contents lists available at ScienceDirect

Cement and Concrete Research

journal homepage: www.elsevier.com/locate/cemconres

Sorption and electrokinetic properties of ASR product and C-S-H: A comparative modelling study

Nicolas Krattiger [a], Barbara Lothenbach [a,b], Sergey V. Churakov [a,c,*]

[a] Institute of Geological Sciences, University of Bern, Baltzerstrasse 1+3, 3012 Bern, Switzerland
[b] Laboratory for Concrete & Construction Chemistry, Swiss Federal Laboratories for Materials Science and Technology (Empa), Ueberlandstrasse 129, 8600 Dübendorf, Switzerland
[c] Laboratory for Waste Management, Paul Scherrer Institute (PSI), Forschungsstrasse 111, 5232 Villigen PSI, Switzerland

ARTICLE INFO

Keywords:
Alkali-silica reaction
Ion adsorption
Monte Carlo simulations
Zeta potential

ABSTRACT

Alkali-silica reaction (ASR) is one of the most important concrete durability issues worldwide. ASR products formed at high temperature have a structure similar to the natural mineral shlykovite. Reactive Grand Canonical Simulations were used to investigate sorption of K^+, Cl^- and Ca^{2+} on C-S-H and ASR products at different pH (10.0 to 13.0) and pore water chemistry. Divalent ions can overcompensate for the negative surface charge, in particular for C-S-H, which leads to a co-adsorption of negative species such as Cl^-. At high K/Ca in solution, monovalent K^+ can desorb calcium from C-S-H and shlykovite surface. The calculated Ca/K partition coefficient shows a higher affinity of ASR product for K^+, while C-S-H favours Ca^{2+}. The uptake of K^+ by ASR products lowers the alkali concentration in the solution and could thus slow down the rate of ASR.

1. Introduction

The alkali-silica reaction (ASR) is one of the most important degradation mechanisms affecting concrete structures worldwide [1,2]. ASR is a chemical reaction within the aggregate with significant volume change, which results in expansion and cracking of the concrete structure [3]. Despite the great number of research studies carried out in the last 80 years, the mechanistic link between chemical reactions and mechanical consequences is poorly understood. Certain minerals in the aggregates can react with the high-pH pore solution of the concrete to form a "gel", as the ASR products are often referred to in literature. Such ASR products consist of alkali, calcium, silica and water with an approximate composition $[(K_2 + Na_2)O]_{0.3–0.9}(CaO)_{0–0.3}[Si_4O_8]\times nH_2O$, where calcium is mainly supplied by the concrete pore solution [4–6]. Various crystalline ASR products such as K-shlykovite and Na-shlykovite have been synthesized in the laboratory at 80 °C [7]. These ASR products have also been observed in concrete samples subjected to accelerated ASR conditions between 60 and 80 °C [8]. The short-range atomic structure of crystalline K(or Na)-ASR products is similar to the structure of the natural mineral shlykovite ($KCa[Si_4O_9(OH)]\cdot 3H_2O$) [7,9,10]. Shlykovite has a layered structure and crystallizes in the monoclinic $P2_1/c$ space group (Fig. 1). The layers of Ca octahedra are located in the rectangular plane $a \times b$ plane with the 2D lattice dimensions 6.51 × 7.04 Å. The layer of Ca octahedra is sandwiched in-between two sheets of Si tetrahedra forming 8-member rings. The center of these rings are occupied by potassium ions. One apical oxygen atom in the 8-member silica ring is represented by an OH group. This OH site is believed to be reactive in contact with electrolyte solution. Whether and to which extent other cations such as K^+, Na^+ or Ca^{2+} could replace H^+ on the OH site is not known, although such a replacement is expected based on the variation in the measured K/Si, Na/Si and Ca/Si ratios on synthesized ASR products [7,11] and ASR products formed in concrete [4].

Calcium silicate hydrate (C-S-H) is the main phase in hydrated Portland cements. C-S-H is a poorly ordered solid phase with a variable Ca/Si ratio depending on the availability of Ca and Si. Its structure can be described assuming a defect tobermorite structure, i.e. a calcium oxide layer with wollastonite type silica chains ("dreierketten" structures, i.e. repeating sequence of three silica tetrahedral) attached to both sides of the Ca layer [12,13]. Two "pairing" tetrahedra are linked to the calcium oxide layer, while a third, bridging tetrahedron (omitted in Fig. 1) links the two pairing tetrahedra [14,15]. Several such sheets form poorly ordered stacks, which are held together by water, interlayer cations (calcium as well as alkalis and other ions) in the interlayer space [16,17]. The deprotonation of the hydroxyl groups on the silica and

* Corresponding author at: Paul Scherrer Institute, Forschungsstrasse 111, 5232 Villigen PSI, Switzerland.
E-mail addresses: nicolas.krattiger@students.unibe.ch (N. Krattiger), barbara.lothenbach@empa.ch (B. Lothenbach), sergey.churakov@geo.unibe.ch (S.V. Churakov).

https://doi.org/10.1016/j.cemconres.2021.106491
Received 13 December 2020; Received in revised form 5 May 2021; Accepted 13 May 2021
Available online 26 May 2021

calcium leads to a negative surface charge, which can be compensated by Na^+ or K^+ or even overcompensated by bivalent cations such as Ca^{2+} [18–20].

The uptake of Na^+ and K^+ on C-S-H lowers, significantly, the alkali concentrations in the surrounding solutions [16,17,21,22] and thus the pH values in the pore solution of the concrete [23,24]. Lower pH conditions slow down the dissolution of the Si-rich aggregates in concrete and thus lower the tendency to form ASR products [25–28]. The uptake of Na^+ and K^+ by C-S-H is suppressed in the presence of high calcium concentrations as well as at high Ca/Si in the C-S-H [16,17,21]. Another important effect is the replacement of alkalis sorbed on the surface of C-S-H by Ca^{2+}. These alkali ions released by C-S-H can then contribute to the formation of ASR product over long times. It has been suggested that the release of alkalis bound in ASR products due to the replacement by Ca^{2+}, which is called "alkali recycling", could be a main factor to drive the continuing formation of ASR at late ages [29,30]. The understanding of the sorption of Ca and alkalis on C-S-H and ASR products and their relative stability is thus of importance for the long-term stability of structures affected by ASR.

The key mechanism responsible for the ion uptake by C-S-H and ASR product is the electrostatic attraction between ions and charged surface sites formed by deprotonation of the silanol groups in alkali solution. As shown in Fig. 1, the C-S-H and ASR product surfaces have very different density of surface silanol groups. Assuming similar hydrolysis constants for these groups on the C-S-H and ASR product surface, the net surface charge density is expected to be very different and therefore lead to different sorption ability and surface electrokinetic properties of both phases as function of pH. These atomic scale differences should result in macroscopically different sorption dynamics and partitioning of Ca and alkali ions between C-S-H and ASR products.

Closely following the modelling approach earlier developed in [19,20,31], we apply reactive Grand Canonical Simulations to investigate the uptake of Ca and alkali ions by the surface of ASR product and C-S-H phases. The model used in this work relies on the explicit treatment of the electrostatic interaction between specific surface sites undergoing to de−/protonation reactions and the finite ion size, whereas the solvent is treated as dielectric continuum. This model provides a mechanistic link between atomic scale structural properties of minerals and their thermodynamic sorption behaviour.

2. Methods

2.1. ASR structural model

The structure of a shlykovite platelet was taken as the basis of structural model for the simulation of ion uptake by ASR product with reactive GCMC. In a similar way, the structure of tobermorite with omitted bridging tetrahedra is considered as structural prototype for C-S-H (Fig. 1).

In the reactive GCMC simulations, the ions are represented by charged hard spheres with a finite size, whereas the solvent molecules are modelled implicitly by homogeneous dielectric continuum with the constant relative permittivity equal to the one of bulk water, $\varepsilon = 78$. All aqueous ions were assumed to have one and the same ionic radius equal to 2.0 Å. This effective radius represents the ion and its hydration shell. The model corresponds to the so-called restricted primitive model of electrolyte and has been successful in predicting thermodynamic properties of electrolyte solutions in a wide range of conditions [33]. The ASR product and C-S-H surfaces are represented by an infinite planar wall containing a rectangular lattice of point lattice sites. These surface sites are distributed according to the location of reactive ≡SiOH groups in the structure of tobermorite and shlykovite. These reactive ≡SiOH surface sites can protonate or deprotonate according to reaction 1.

$$\equiv \mathrm{Si(OH)^0} + \mathrm{H_2O} \leftrightarrow \equiv \mathrm{SiO^-} + \mathrm{H_3O^+} \quad (1)$$

The corresponding equilibrium constants are set to $pK_a = 9.8$, which is the first protonation constant of silicic acid in aqueous solution. The details of the simulation algorithm and the statistical mechanics

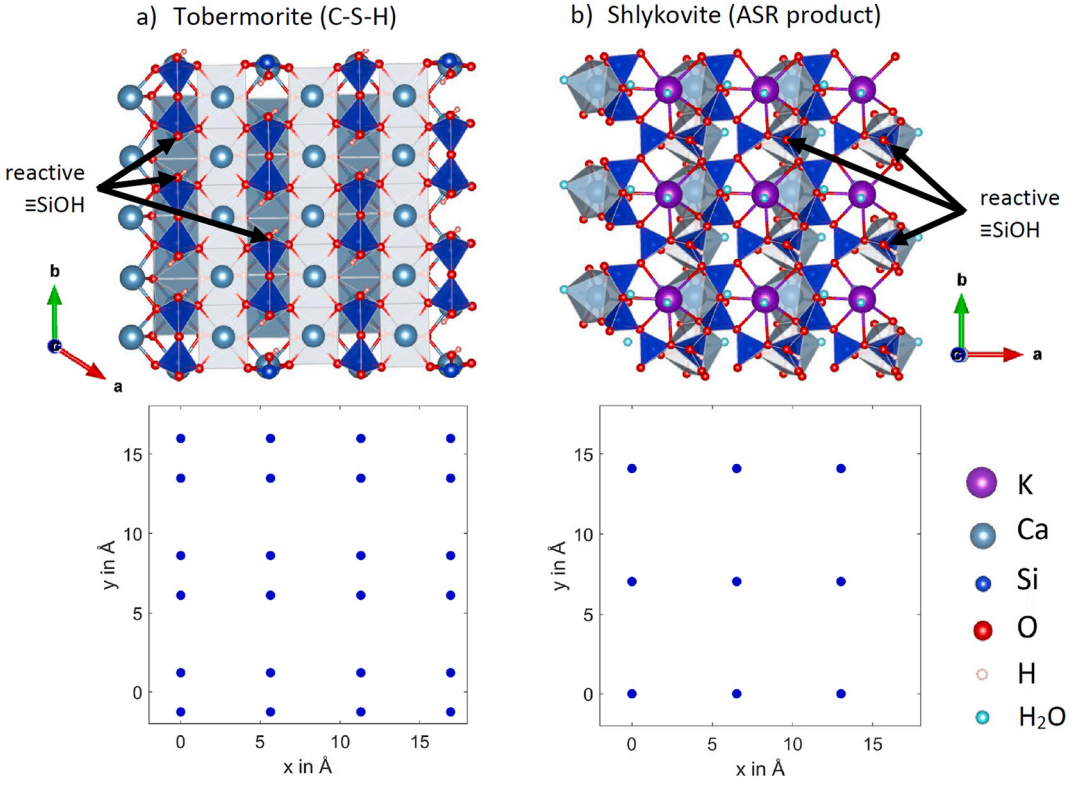

Fig. 1. Structure of natural mineral shlykovite (from [7,32]), tobermorite [12] with omitted bridging tetrahedra (top), and the model representation of ASR product and C-S-H in the GCMC simulations (bottom) as a set of point sized titratable silanol groups with site densities of 2.2 and 4.8 nm^{-2}, respectively.

background are described elsewhere [19,20,22,34].

2.2. System setup in GCMC

The reactive bridging tetrahedra in the tobermorite structure [12] are distributed on a 2D regular rectangular mesh with 5.65 × 7.36 Å^2 lattice dimensions. The average surface site density for the C-S-H model is 4.82 sites nm^{-2}, identical to our previous simulations [20,22]. The reactive surface sites in the shlykovite structure are also located on a rectangular grid with the surface site density 2.18 sites nm^{-2}.

Equilibrium distribution of ions and the protonation state of the C-S-H surface is obtained by Monte Carlo simulations in the Grand Canonical ensemble (i.e., constant chemical potential, volume and temperature), using the standard Metropolis algorithm. In addition to the conventional GCMC insertion/deletion of ion pairs in the simulation box, the surface sites were allowed to titrate according to the reaction in Eq. (1). The deprotonation of the surface sites corresponds to a change of their charge state from "0" to "-1".

The simulation boxes for ASR product and C-S-H had 130 × 141 × 200 Å^3 and 181 × 177 × 200 Å^3 dimensions, respectively, with an exception of the titration experiment in $Ca(OH)_2$ at pH 10.0 and 10.5, where a bigger 500 Å long box normal to the surface was used to accurately represent diffuse double layers. The simulated ASR product and C-S-H surfaces comprise 400 and 1536 lattice sites respectively. The long-range electrostatic interaction was treated using charge sheet model [35].

Ion profiles and the electrostatic potentials in the system were obtained by averaging the atomic configurations from at least 500′000 MC cycles. Each particle in the system is attempted to move within the MC cycles. At least 10% of the MC cycles included the GCMC steps attempting insertion/deflection of the ions in the system and de-re-protonation of the surface sites. Prior the production runs each system was equilibrated until the thermodynamic parameters (e.g. energy and composition) fluctuated around a constant mean value. The statistical variance of the results was estimated using block averaging.

The adsorption properties of ASR product and C-S-H were investigated for several systems containing mono and divalent cations in a range of pH between 10 and 13.0: in pure $Ca(OH)_2$ solution, in a mixture of KOH and $CaCl_2$ with constant calcium concentration of 2 and 20 mM, and in a mixture of KOH with 0.5 KCl and 0.1 KCl solution. In each simulation, the corresponding base concentration was adjusted to maintain the required pH of the bulk electrolyte solution, the possible precipitation of portlandite, and of C-S-H in the case of ASR product, was not taken into account. The chemical potentials of ions for GCMC simulation were calculated in a separate set of simulations of bulk electrolyte using modified Widom particle insertion method for electrolyte solutions [36].

The excess surface adsorption of cations and anions at the interface was calculated according to Eq. (2).

$$S(L) = \int_0^L (c(x) - c_0)\, dx \tag{2}$$

In practical calculations, the box size is selected big enough that the bulk electrolyte concentration c_0 is reached well within the box boundaries. It is important to realise that if the concentrations throughout the domain were constant and equal to the concentrations of the bulk electrolyte solution, the calculated adsorption for ions of finite size would have been negative, according to the Eq. (2). This is because the ions of finite size have a maximal approach distance, resulting in an exclusion volume near the surface. A positive value of the sorption suggests that the ion depletion in the exclusion volume is over-compensated by the ion accumulation at the interface above the concentration of the bulk electrolyte.

Partitioning of Ca and K between ASR and C-S-H is described by the exchange reaction (Eq. (3)) and the corresponding partitioning coefficient (Eq. (4)). Knowing the total concentration of the adsorbed potassium and calcium ions at the ASR product and C-S-H surfaces the thermodynamic partition coefficient can be calculated.

$$[\mathrm{Ca}]_{\mathrm{ASR}} + [\mathrm{K}]_{\mathrm{C-S-H}} = [\mathrm{K}]_{\mathrm{ASR}} + [\mathrm{Ca}]_{\mathrm{C-S-H}} \tag{3}$$

$$K_D = \frac{[\mathrm{Ca}]_{\mathrm{C-S-H}}}{[\mathrm{K}]_{\mathrm{C-S-H}}} : \frac{[\mathrm{Ca}]_{\mathrm{ASR}}}{[\mathrm{K}]_{\mathrm{ASR}}} \tag{4}$$

To obtain the total amount of ions adsorbed, we assume that the ion within the shear plane defined to be at 1.5 ion diameters to the surface belong to the surface. The total concentration of the ions adsorbed is calculated using Eq. (5).

$$[\mathrm{X}]_{\mathrm{solid}} = \int_0^{L_\zeta} c_{\mathrm{X,aq}}(x)\, dx \tag{5}$$

where $[X]_{\mathrm{solid}}$ corresponds to the total amounts of adsorbed Ca or K on C-S-H or ASR product in Eqs. (3) and (4) and L_ζ is the position of the shear plane.

2.3. Simulation uncertainties and model assumptions

The models used in this study are based on a number of approximations and assumptions, which need to be considered while interpreting the results. The ions are represented by charged hard spheres and the solvent is treated as dielectric continuum. All electrolyte species have the identical ion radii. Within this approximation, any ionic species carrying the same charge are indistinguishable. For example, OH^- groups and Cl^- ions appeared to have identical interaction potential with the other species in the system. In principle, ion specific interactions could be incorporated into the model adding dedicated short-range interaction potential. These parameters could be tuned either to reproduce ions specific structural properties, e.g. distance of closest approach or ion-ion pair correlation function, or to reproduce thermodynamic properties of bulk electrolytes. The main aim of this study was, however, to discriminate the specific effect of ionic charge and to compare the behaviour of the system dominated by Ca and K. For this reason, the hard radii were selected for both ions (2.0 Å). This value corresponds approximately to the arithmetic mean of the radii for KCl (d = 1.63 Å) and $CaCl_2$ (d = 2.38 Å) system derived to reproduce the thermodynamic properties of corresponding binary electrolytes [37]. Compared to the ion specific parameters, the ones used in our study predict weaker interaction for the K-X^- and stronger interaction for Ca-X^- (X^- = OH^-,Cl^-, ≡SiO^-). Accordingly, it can be expected that the corresponding ion specific parameters would predict smaller differences between the behaviour of K^+ and Ca^{2+} dominant systems. Thus, the simulations reported in this study provide estimate of the maximal effect to be expected in K^+ and Ca^{2+} pure and mixed electrolyte systems.

The use of the dielectric continuum approximation smears out the short-range directional interaction between the ions and the solvent molecules. Such steric effects could be relevant for the stabilisation of specific geometry of the surface adsorbed ions by their coordination shell and hydrogen bonding interaction between the hydration shell molecule and the HB acceptor on the mineral surface. The specific steric interaction of ions with the surface can emerge when the ion dimension matches a specific structural topology at the mineral surface. Depending on the strength of the ion-solvent and ion-surface interaction, ions form either outer- or inner-sphere surface complexes. In the GCMC model used in this study, the sorption sites are assumed to have a point size. This assumption implies that the contact of closest approach to the surface sites corresponds to the inner-sphere surface complexes.

Another source of uncertainties is the assignment of the intrinsic pK_a value to the surface silanol sites. Recent ab initio simulations have shown that the acidity of silanol groups may depend strongly on the local environment [20,38–40]. For C-S-H, the ab initio derived acidities of the silanol groups range from 6.15 to 11.83 pK units. The sensitivity of

the C-S-H surface charge and its electrokinetic properties with respect to the acidity of the silanol groups was investigated by previous studies [20]. The GCMC simulations have shown that at pH above 10 (e.g. in the range of the C-S-H stability) the predicted properties of C-S-H obtained with ab initio derived acidity constants are well comparable with the ones obtained assuming that all the surface silanol groups have the same acidy equal to the first hydrolysis constant of silicic acid [20]. Earlier studies of C-S-H and other silicate minerals with GCMC method further confirm that simple models considering only one type of silanol group on the surface can successfully reproduce the experimental data [19,22,41,42]. The intrinsic acidity of the silanol groups at the ASR surface is not known. Without having any better estimate for ASR and for the sake of model simplicity we assume that the acidity of the silanol group in C-S-H and ASR is the same and equal to pK = 9.8. Despite its simplicity, this model was found to reproduce experimental data for C-S-H by molecular simulation over a wide range of experimental conditions [22].

The GCMC model applied in the simulations does not consider the dissolution precipitation phenomena, apart from the protonation-deprotonation reactions. It is known that the Ca:Si ratio at the C-S-H depend on the pH and Ca concentration in the solution [14,15]. Considering the tobermorite structure as the reference for C-S-H model, the chain of Si-tetrahedra becomes de-polymerised at higher pH. These leaching process is not considered in the applied GCMC model. Fortunately, the leaching of Si from the C-S-H surface do not change the surface site density of the silanol groups, and can be neglected in the simulation of ion adsorption and the surface charge density within the applied GCMC model.

3. Results & discussion

3.1. Titration/surface charge

This work aims to compare C-S-H and ASR product in different chemical environments. It is known that the presence of Ca^{2+} in the electrolyte solution has the most prominent effect on the electrokinetic properties and the surface charge of C-S-H [22]. A first set of simulations was conducted in the pure $Ca(OH)_2$ system. The calcium concentrations were adjusted by titrating with $Ca(OH)_2$, $5{\cdot}10^{-5}$ to $5{\cdot}10^{-2}$ mol/L, to model pH-conditions in the range from 10.0 to 13.0. The possible precipitation of portlandite at pH 12.5 and above was suppressed in the model calculations. The evolution of surface charge density and the fraction of deprotonated surface sites as function of pH is shown in Fig. 2a. If the fraction of the protonated sites is considered, the advance of deprotonation with pH is more efficient on the ASR product surface compared to C-S-H. Only 60% of the surface sites on C-S-H are deprotonated at pH 11.5, whereas nearly 80% of the sites are deprotonated on ASR product at the same conditions.

The lower deprotonation of the surface sites on C-S-H compared to ASR product at a given pH (if expressed as surface site fraction) is related to the differences in the surface charge density of the two phases. The ability of the surface site to deprotonate is modulated by the electrostatic repulsion among the deprotonated sites. At low surface site density, the repulsion is less pronounced. Calculations show that for a given pH and electrolyte concentration, the fraction of the de-protonated surface sites is always higher for the ASR product. This effect is shown in Fig. 2b. If the deprotonated surface sites were not interacting electrostatically with each other, the deprotonation would follow the titration curve of an isolated molecule of silicic acid in solution ($pKa_1 = 9.8$). The higher the site density the stronger is the site-site electrostatic interaction and accordingly the lower is the increase of the fraction of deprotonated sites as a function of pH.

Alternatively, the steepness of the slope at which absolute surface charge density increases in two phases as function of pH can be compared. The site density of C-S-H is nearly 2 times larger than that of ASR product. Accordingly, the absolute value the surface charge density of the C-S-H is always higher compared to the ASR surface. Therefore, the titration curve for the surface charge density is substantially steeper for ASR, whereas the C-S-H surface charge density is building up more slowly. This observation is related to the fact that ASR surface sites are less affected by the protonation state of neighbouring sites and the obtained titration curve is closer to the one expected for a molecule of silicic acid in solution at infinite dilution. This effect is again underlined in Fig. 2b, showing that the titration curves for C-S-H are flatter than the ones for the ASR product.

Similar comparative behaviour of surface charge density and the fraction of deprotonated sites in ASR product and C-S-H is observed for different compositions of background electrolytes (Fig. 2a). In general, the Ca ions are known to promote the deprotonation reaction of ≡SiOH groups by strong screening of the charged surface sites as illustrated clearly in Fig. 2a, where at pH 10 the fraction of deprotonated surface sites increases with the calcium concentration. The simulations performed in 20 mM background $CaCl_2$ solution suggest the most efficient build-up of the surface charge for both ASR and C-S-H systems. Thus, nearly 90% of the surface sites are deprotonated on ASR product and 70% of the sites for C-S-H at pH 11.5.

The titration in 2 mM background $CaCl_2$ solution shows less efficient deprotonation than in the 20 mM solution, due to a lower screening of the deprotonated surface sites. At pH 11.5, nearly 80% of the surface sites on ASR product and 60% of the sites on C-S-H are deprotonated.

Compared to the Ca rich system, the deprotonation is less efficient in the KCl system, in 0.1/0.5 KCl solution 50/70% of the surface sites on ASR product are deprotonated at pH 11.5 and only 30/40% on C-S-H. In both ASR product and C-S-H systems the surface charge increases quasilinear with pH. It is interesting to note that the absolute surface charge density in the system with monovalent cations is rather close for both ASR product and C-S-H in the entire pH range. This behaviour is clearly different to the observation for the Ca dominated electrolytes, where Ca has much more influence on deprotonation on C-S-H than on ASR product. Such an effect has been described and discussed by Labbez et al. in the systematic GCMC study of the electrokinetic properties of surfaces as function of surface site density and the electrolyte composition [31].

3.2. Cations adsorption

The diagrams on the left compare cation adsorption in units of number of cations per nm^2, on the right units of number of adsorbed cations per SiOH surface site were used.

The adsorption of monovalent and divalent ions on ASR and C-S-H surface as a function of pH is shown in Fig. 3a. The sorption trends are qualitatively different on C-S-H and ASR product. On C-S-H the adsorption shows overall a linear trend for monovalent cations as a function of pH. The trend is also linear for divalent cations up to pH 12.0 and then starts to flatten out. In general, the difference between the monovalent and divalent cations is not very large in units of #cations per nm^2 or per surface site (Fig. 3a top). This relatively small difference can be translated into a corresponding shift in pH by approximately 0.5 units. The observed amount of adsorbed ions increases from 0.5 ions/nm^2 at pH 10 to nearly 2.7 ions/nm^2 at pH 13.0.

The cation sorption behaviour is distinctly different on ASR product. The adsorption of divalent cations such as Ca^{2+} increases linearly with the pH up to pH 11.5. At higher pH values, the sorption of divalent cations flattens out at a value slightly above 1.1 cations/nm^2. In contrast, the adsorption of monovalent cations linearly increases up to the pH of about 12.5 and levels off at higher pH. This behaviour is explained by the lower surface site density in ASR product and the evolution of the surface charge as a function of pH (see Fig. 2a). The maximal surface site density and the surface charge on ASR product is 2.2 charge equivalents/nm^2. The sorption levels off for divalent cations at ~1.1 sites/nm^2; this translates into a charge equivalent concentration of 2.2 e/nm^2, which is very close to the surface site density on ASR product (Fig. 3a bottom). Nearly all surface sites are deprotonated on

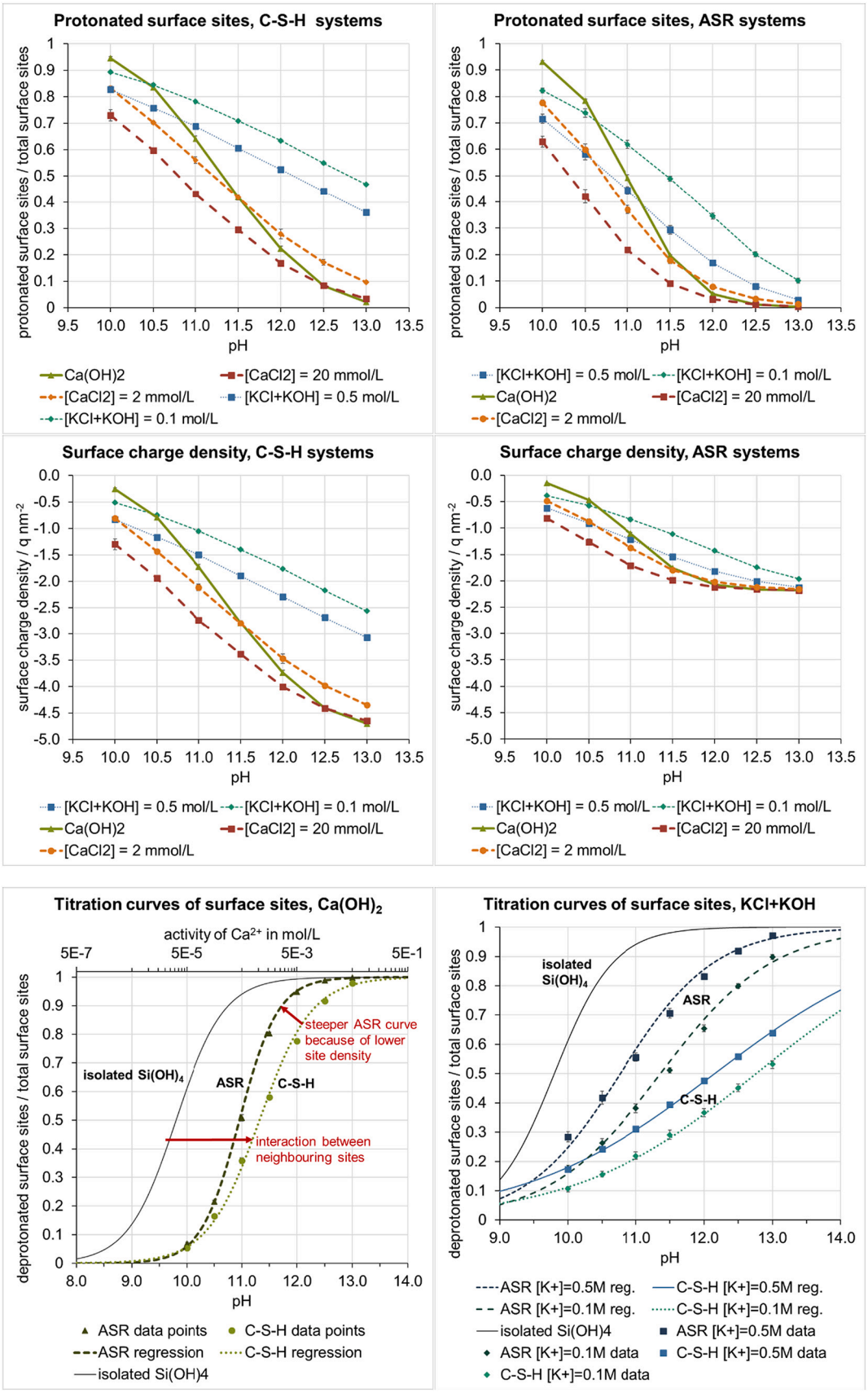

Fig. 2. a. Fraction of protonated sites (top) and the surface charge density (bottom) as function of pH in C-S-H and ASR product.
b. Fraction of deprotonated sites for pure Ca systems (left) and pure K systems (right) in comparison with the theoretical titration curve for an isolated $Si(OH)_4$ in solution (solid line). Data points are interpolated by a least square regression of a model function $(1 + 10^{a \cdot \mathrm{pKa} - b \cdot \mathrm{pH}})^{-1}$ (dotted lines). The minor discrepancies between the model fit and the data points are explained by the model simplicity.

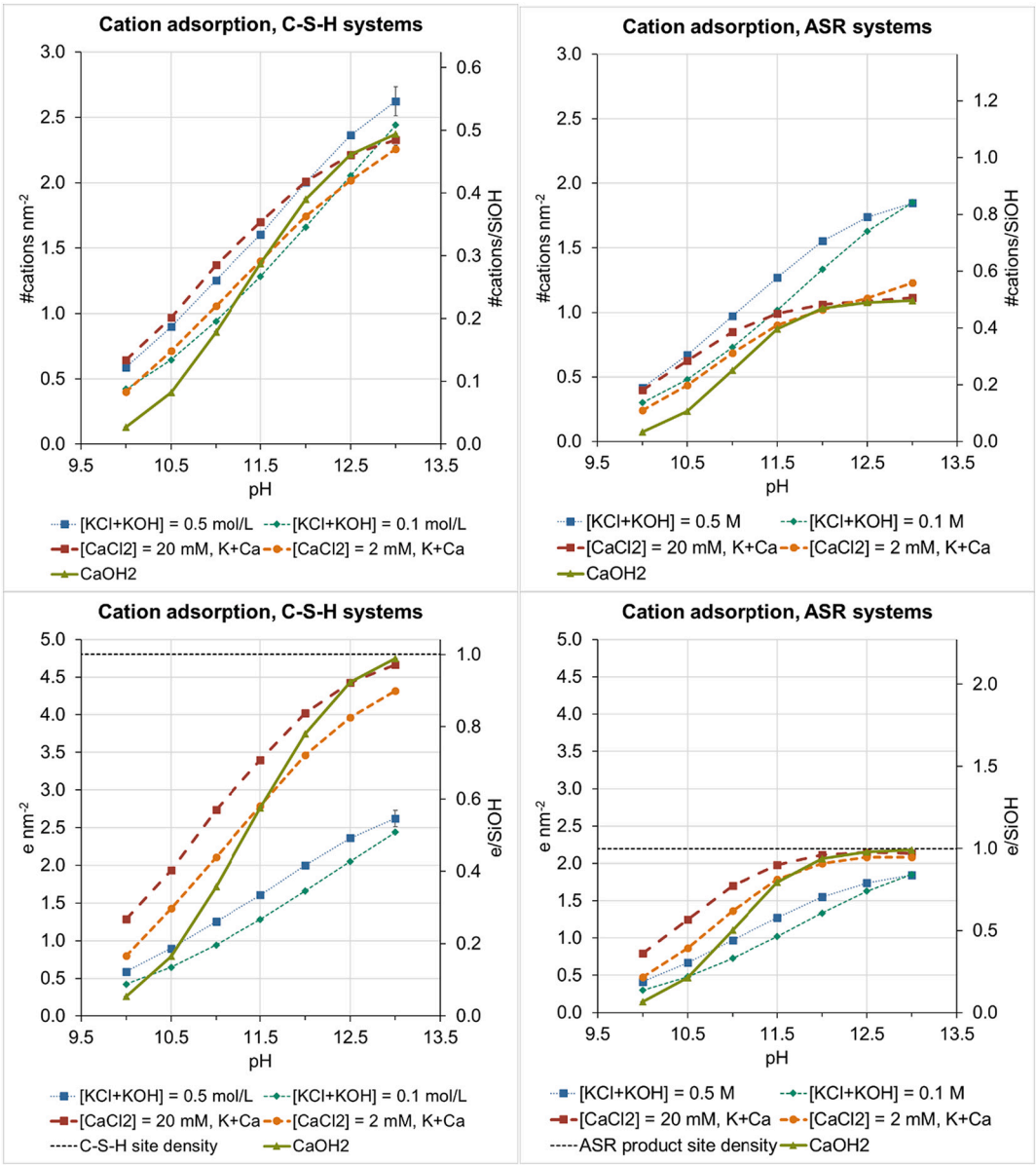

Fig. 3. a. Adsorption of positively charged species on C-S-H and ASR product respectively in units of #cations nm^{-2} and #cations/SiOH (top) and in units of charge equivalents e nm^{-2} and e/SiOH (bottom).
b. Top: direct comparison of cation adsorption on C-S-H (y-axis) and ASR surface (x-axis). Bottom: ratio of cation adsorption on C-S-H and cation adsorption on ASR product as a function of pH. The dotted lines indicate equipartitioning of cations between either phase.

ASR surface at pH above 11.5 and the sorption capacity of ASR product is consumed. A doubled amount of monovalent cations is necessary to compensate the surface charge in the system dominated by monovalent ions, i.e. K^+. In addition, the surface charge evolution of the surface charge Fig. 2a shows that the complete deprotonation of the surface sites in the 0.5 M KCl solution is achieved at pH 13.0.

A maximum cation uptake of 0.5 Ca^{2+} or ≈0.6 K^+ per ≡SiOH surface site on C-S-H is calculated at pH 13, which translates into a maximum Ca/Si_{tot} of 0.17 and K/Si_{tot} of 0.2, if normalised to all Si groups in C-S-H. This calculated alkali uptake agrees well with 0.2 to 0.3 K/Si_{tot} measured at 0.1 M KOH solutions [16,17] and also to the measured cation exchange in C-S-H [43]. For the ASR product, where 1 ≡ SiOH surface site per 4 silica groups is present, a maximum cation uptake of 0.5 Ca^{2+} or ≈0.8 K^+ per ≡SiOH surface site is obtained, indicating that the ASR product can contain more K and Ca than the mineral shlykovite ($KCa[Si_4O_9(OH)]\cdot 3H_2O$) resulting in compositions in the range of $K_{1.8}Ca[Si_4O_9(OH_{0.2})]\cdot 3H_2O$) to $KCa_{1.5}[Si_4O_9(O)]\cdot 3H_2O$) or total $K/Si_{tot} = 0.25$ to 0.5 and $Ca/Si_{tot} = 0.25$ to 0.38. In systems where ASR products form experimentally, low calcium concentration (0.01 to 1 mM Ca in synthesized lab samples [5,7]) and relatively high K concentration (≈500 mM) are present, i.e. conditions comparable to the calculation [KCl + KOH] = 0.5, such that mainly an increase of the alkali content can be expected. In fact, (K + Na)/Si in the range of 0.2 to 0.5 and Ca/Si of ≈0.2 to 0.3 are reported for synthetic ASR products and in field samples [4,5,8,11,30]. At higher Ca concentrations, ASR products would be destabilised to C-S-H in experiments [5]; this was supressed in the calculations here, to be able to study and compare a more complete range of conditions.

In Fig. 3b (top) the cation adsorption on C-S-H surface is directly plotted against the cation adsorption on ASR product to enable direct comparison. The left part of the figure shows that for a given pH more cations will absorb per unit surface area of C-S-H compared to ASR

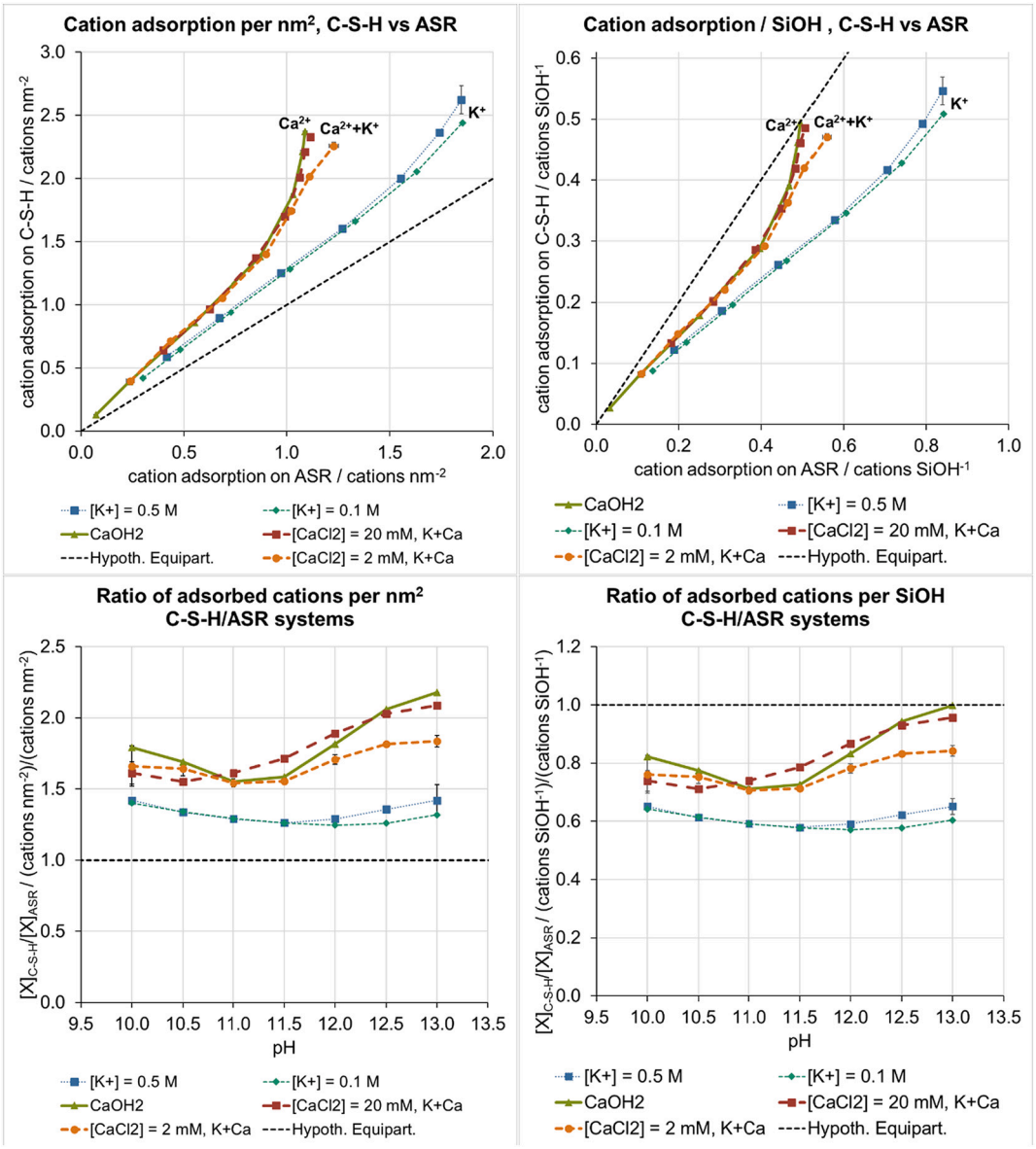

Fig. 3. (*continued*).

product, if both ASR and C-S-H are brought into equilibrium. This is because C-S-H has a higher surface charge density than ASR product at the same pH conditions; the dotted line shows hypothetical equi-partitioning. In the diagram on the right the same cation adsorption data are normalised by the number of cations per reactive ≡SiOH surface site. Again, the dotted line indicates equipartitioning. For a given pH, the density of adsorbed cations per silica surface site is higher on ASR product compared to C-S-H because the fraction of deprotonated surface sites at a given pH is higher on ASR product. Even though the number of cations absorbed per surface site is higher on ASR product, the total cation adsorption on C-S-H is still larger because the surface site density and the surface charge density are higher on C-S-H. This effect becomes clearer if we look at the plots of the KCl systems in Fig. 3b (bottom left). The ratio of adsorbed cations per nm^2 on C-S-H and on ASR product is about 1.3 on average in the pure alkali systems. At the same time, there are approximately two times more negatively charged surface sites per unit area on C-S-H than on ASR product due to the differences in silanol density (if we assume all silanol groups to be deprotonated). So in the case of C-S-H, the factor of 1.3 times higher cation adsorption per unit area divides by a factor of two due to the higher surface site density. This leads to a value of ~0.65 for the ratio of adsorbed cations per silanol on C-S-H and on ASR product, as can be observed in Fig. 3b (bottom right).

Fig. 3b (top) also shows that Ca has stronger affinity towards C-S-H surfaces compared to K. This effect can be shown even better if we consider the ratio of absorbed cations on C-S-H and absorbed cations on ASR surfaces as a function of pH (Fig. 3b bottom). This ratio can be interpreted as a partition coefficient between the two solids. The higher the value, the higher the affinity of cation to C-S-H with relation to ASR product. A value greater than 1 means overall preferred adsorption on C-S-H. The partition coefficients for Ca are about 30 to 50% higher than for K, which underlines the strong affinity of Ca for C-S-H or, in other words, the stronger ability of C-S-H for attracting divalent cations vs mono-valent cations such as K^+.

3.3. Anions adsorption

The anion adsorption calculated with Eq. (2) is shown in Fig. 4. For the system with monovalent cations, K^+, the adsorption value for anions is negative in the entire pH range, indicating an anion exclusion. The corresponding concentration profiles are reported in supplementary

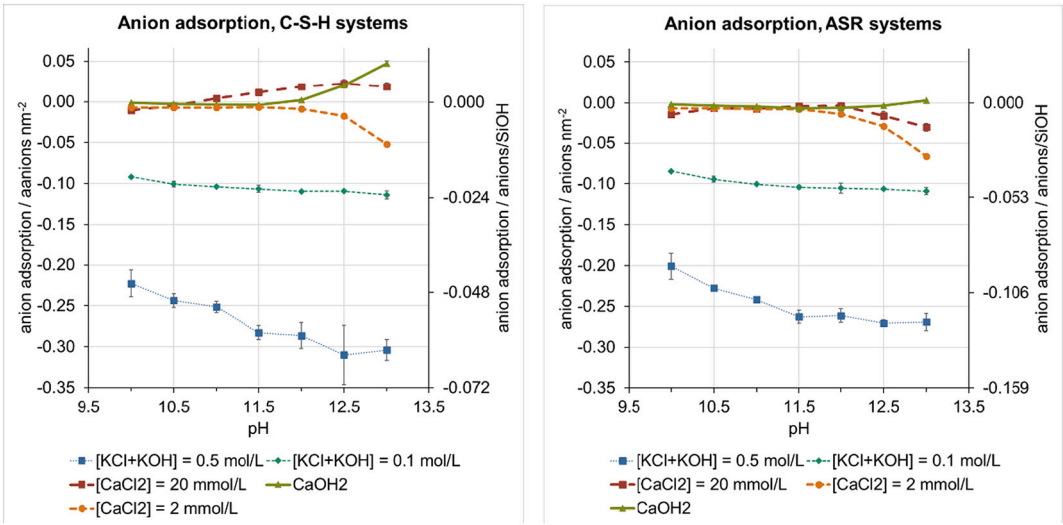

Fig. 4. Adsorption of negatively charged species on C-S-H and ASR product respectively. Negative values indicate anion exclusion from the surface.

materials. Remarkably, the predicted values of the anion exclusion in the presence of K^+ for ASR product and C-S-H are very similar and show very weak dependency on pH.

In the presence of Ca^{2+}, a limited anion adsorption on C-S-H is predicted at higher Ca^{2+} concentrations and pH values. In the pure Ca $(OH)_2$ system, the calculated anion adsorption is close to zero and turns slightly positive at pH above 12.0. The pH dependence of anion adsorption in 20 mM $CaCl_2$ system is a bit more complex. On C-S-H the excess anion adsorption is positive above 10.5 and increases linearly at intermediate pH and changes to decreasing trend above the pH 12.5. These calculated trends are in agreement with experimental observations on C-S-H in the presence of $CaCl_2$, where weak co-sorption of monovalent anions has been measured [44]. On ASR product, the anion adsorption is slightly negative to close to zero in the range of pH from 10.0 to 12.5 and decreases prominently above pH 12.5. The observed behaviour of ASR product and C-S-H in 2:1 electrolyte is the combined result of the anion exclusion at the negatively charged surface and the co-adsorption of the monovalent anions with the divalent cations covering the mineral surface. The concentration profiles supporting this interpretation are provided in supplementary materials. These profiles show that in either systems anions are excluded from the first 5 Å (C-S-H) and 6 Å (ASR product) to the surface due to the strong electrostatic repulsion. We defined ions to be excluded in the range where the local density is lower than the bulk concentration. However, a local maximum showing an excess of the anion is observed at the distance 7 Å and 8 Å, respectively. Smaller exclusion volume at C-S-H surface compared to ASR indicates more efficient screening of surface charge by cations. This maximum superimposes with the local minimum on the density profiles of the Ca ions.

For the pure $Ca(OH)_2$ system, the calculated anion adsorption in the range of pH up to pH = 12.0 is close to zero, for both ASR product and C-S-H. At higher pH values, the anion adsorption increases and becomes slightly positive. This indicates that a significant amount of anions accumulates at the interface and compensates for the steric exclusion of cations and anions from the surface due to the finite ions size. The concentration profiles providing clear indication for the co-adsorption of anions are reported in supplementary materials.

The behaviour of the ASR product in pure $Ca(OH)_2$ and $CaCl_2$ + KOH solution becomes qualitatively different above pH 12.5 (Fig. 4). In the former system, the value of the anion adsorption is close to zero or slightly positive and increases linearly with pH and Ca^{2+} concentration. In equilibrium with 20 mM $CaCl_2$ solution, anion adsorption is close to zero up to pH 12.5. At higher pH, the anion adsorption decreases to strongly negative values. In 2 mM $CaCl_2$ solution, the decrease in excess adsorption starts already at pH 12. The origin of this effect is explained by the competing effect of anion exclusion and co-adsorption. It is important to realise that the calculated 'zero' excess adsorption of anions indicates a weak enrichment of the anions at the interface, which is compensating the steric exclusion of anions due to the final ionic size and electrostatic anion repulsion of anions from the negatively charged surface. This enrichment is controlled by co-adsorption (ion pairing) of anions with Ca^{2+} ions adsorbed on the negatively charged surface. This effect is responsible for the steady increase of excess anion adsorption in the $Ca(OH)_2$ system, where the Ca concentrations increase with pH. In the mixed system ($CaCl_2$ + KOH) the concentration of base (KOH) at high pH becomes comparable, or even higher than the concentration of the background electrolyte $CaCl_2$. At these conditions, K^+ is competing with Ca^{2+} for the sorption sites and causes desorption of Ca^{2+} from the surface (see Fig. 5). Accordingly, the de-sorption of Ca^{2+} leads to decrease of co-adsorbed Cl^- ions. It can be concluded that K^+-rich or highly alkaline solution promote de-sorption of Ca^{2+} from the ASR product surface in general. Such a sorption competition effect is also qualitatively present on C-S-H but becomes relevant only at very high concentration of monovalent cation or in systems with relatively low Ca concentrations (2 mM). Furthermore the de-sorption of Ca^{2+} from C-S-H is energetically less favourable due to the higher surface charge density of the C-S-H surface. In fact, experimentally significant replacement of Ca^{2+} sorbed on C-S-H by K^+ or Na^+ has been observed only at significantly higher Na^+ and K^+ than Ca^{2+} concentrations [17]; no such experimental sorption data are available for ASR product.

3.4. ζ-Potential

Finally, we discuss the electrokinetic properties of C-S-H and ASR systems. The ζ-potential is calculated as the value of the electrostatic potential at the distance to the surface corresponding to 3 ionic radii, which can be related to the position of the shear plane [22]. The electrostatic potentials are reported in supplementary material. The overall qualitative behaviour of ζ-potential on C-S-H and ASR product has a number of similarities (Fig. 6). The ζ-potential is negative and decreasing with increasing pH in the system with monovalent electrolyte solution. In $Ca(OH)_2$ system the apparent surface charge monotonically increases with pH. The simulations predict the charge reversal to occur on ASR and C-S-H surfaces at pH 12.5 and 12.0, respectively, due to the accumulation of Ca^{2+} near the surface. In the 20 mM $CaCl_2$ system the C-S-H has positive potential in the range of pH from 11.0 to 12.8, whereas ASR product is slightly negative nearly in the entire pH domain studied, illustrating again the lower affinity of Ca to ASR

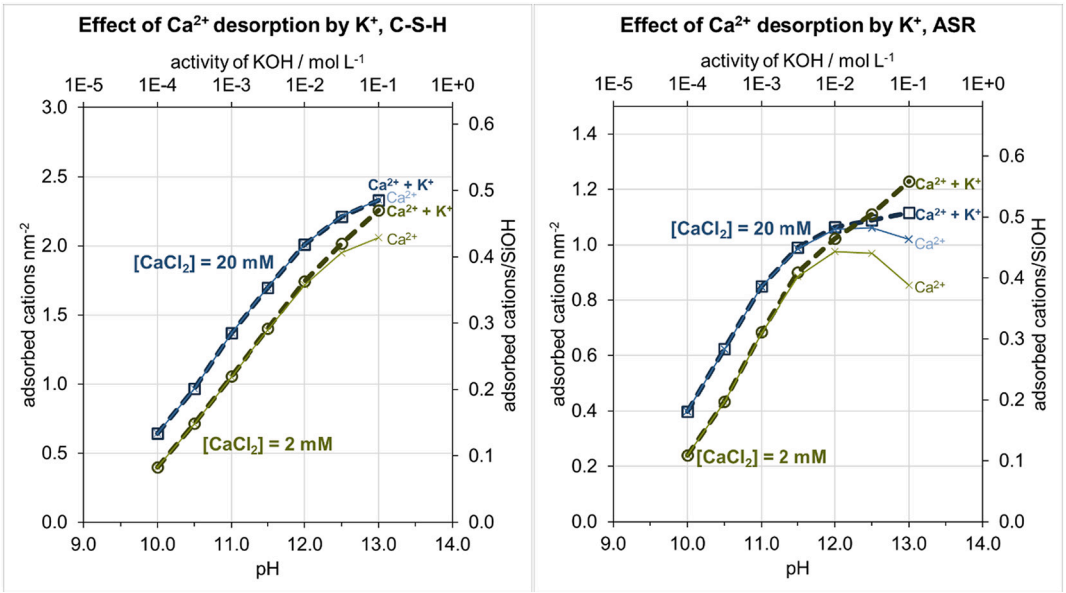

Fig. 5. Comparative sorption behaviour of Ca and K in C-S-H and ASR product as a function of pH controlled by the addition of KOH. For each system, "Ca + K" adsorbed and "Ca" are plotted. Amount of "K" adsorbed is the difference between "Ca + K" and "Ca" curves for each system.

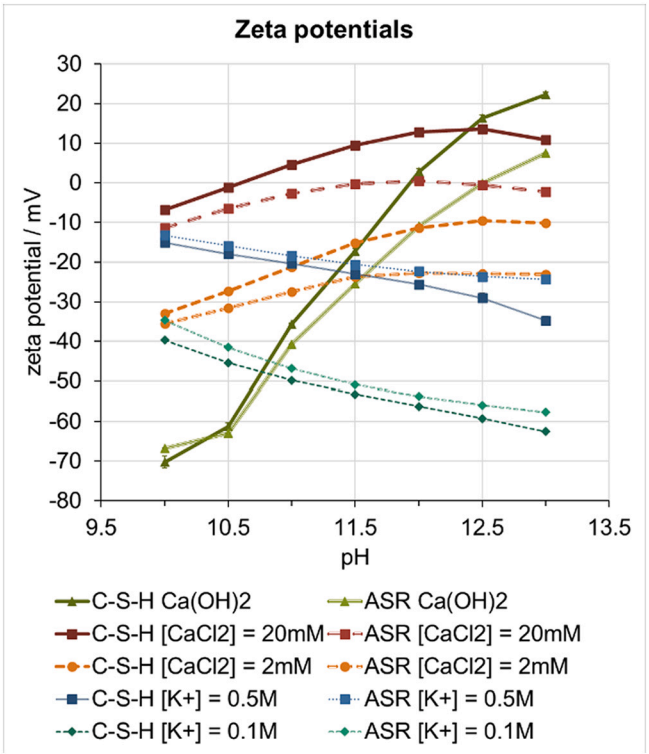

Fig. 6. Evolution of ζ-potential in C-S-H and ASR product as a function of pH in different electrolytes.

product. In 2 mM $CaCl_2$ system, the potential is negative for all considered pH values on both C-S-H and ASR product, with a local maximum at pH 12.5.

In KCl systems, the behaviour of both ASR product and C-S-H is qualitatively similar. Both systems are expected to have more negative ζ-potential at higher pH values due to the progressive de-protonation of the ≡SiOH groups. At higher ionic strength (0.5 M KCl), less negative values of the ζ-potential are calculated. The charge reversal in the presence of higher calcium concentrations as well as the decrease of zeta potential with increasing pH agrees with experimental and simulated zeta potential of C-S-H as detailed in [16,19,22,45]. For ASR product no experimentally determined zeta potential data have been reported in the literature so far.

4. Conclusions

In this work, we apply the primitive model of electrolyte to study titration and sorption behaviour of ASR product in Ca^{2+} and K^{+}-rich electrolytes and compare the simulation results with the behaviour of the most common cement phase, C-S-H. Both, C-S-H and ASR products have a negatively charged surface and thus preferentially adsorb cations at their surface; their surface charges become more negative at higher pH values due to the deprotonation of the ≡SiOH surface sites. The comparative study of C-S-H and ASR product shows that differences in the surface sites protonation state, evolution of surface charge and the ion adsorption as function of pH is largely determined by the distinct surface site densities in both phases. The density of the titratable ≡SiOH surface sites on C-S-H is nearly two times larger than that of ASR product. Accordingly, the highest expected surface charge of the C-S-H surface (e.g. 100% deprotonation of surface sites) is two times the maximum surface charge density expected for ASR product. Since the ion adsorption is primary driven by electrostatic interaction of ions with the charged surface sites, the C-S-H has higher sorption capacity than ASR product. At equilibrium with the same electrolyte solution C-S-H adsorbs more cations and anions per unit of surface area than ASR product.

The higher surface site density of C-S-H leads to stronger electrostatic site-site interactions [22] such that deprotonation is shifted to a higher pH value. Thus 90% deprotonation of ASR product and C-S-H in a pure $Ca(OH)_2$ electrolyte is achieved at pH 11.7 and 12.3, respectively. Divalent cations (e.g. Ca^{2+}) have a stronger ability to promote the deprotonation of the surface sites and higher affinity to the surface than monovalent cations such as K^{+}. Monovalent cations can compete with the divalent ones for the sorption sites, if present in excess and if nearly all surface sites are in deprotonated state. Ca^{2+} ions can be desorbed from ASR product at highly alkaline conditions more easily than from C-S-H because ASR product has lower surface charge density. It is worth emphasis that in both systems the competition becomes significant first at the condition corresponding to nearly complete deprotonation of

surface sites, which onset takes place in ASR product at lower pH conditions. This also emphasises the dominance of divalent cation in controlling the deprotonation reactions on the surface. The calculated Ca/K partition coefficient (Fig. 7) shows that K^+ has a higher affinity to ASR product while Ca^{2+} has a higher affinity to C-S-H. At low pH condition up to pH 11.0–11.5, the preferential partitioning of Ca to C-S-H and K to ASR is independent of pH. At higher pH the preferential partitioning of Ca to C-S-H and K to ASR linearly increases with pH.

This study has also shown that shlykovite, our proxy for ASR products, can be expected to bind K^+ and Ca^{2+}, in addition to the K and Ca in its main layer, leading to solid phase compositions in the range of $K_{1.8}Ca[Si_4O_9(OH_{0.2})]\cdot 3H_2O$ to $KCa_{1.5}[Si_4O_9(O)]\cdot 3H_2O$ or total $K/Si_{tot} = 0.25$ to 0.5 and $Ca/Si_{tot} = 0.25$ to 0.38, which corresponds to the variations in the alkali content observed for synthesized ASR products and observed in field samples [10].

The sorption of Ca^{2+} at the surface can result in a charge reversal at the surface [22]. The co-adsorption of anions (e.g. Cl^-) is thus controlled by the uptake of Ca^{2+} ions on the surface of both phases. Since C-S-H has a higher Ca^{2+} uptake capability and a higher affinity for Ca^{2+}, larger quantities of Cl are co-adsorbed on C-S-H than on ASR product.

The model used in this study suggests that the ζ-potential of the ASR product remains weakly negative at the most relevant conditions. A close to zero value of ζ-potential is predicted for the system in equilibrium with 20 mM $CaCl_2$ in a wide range of pH. Modelling also predicts a possibility of charge reversal in ASR product-$Ca(OH)_2$ system at pH above 12.5. Note that ASR product is expected to be less stable than C-S-H at high Ca concentrations [5]. For comparison, C-S-H is expected to have positive surface charge in the 20 mM $CaCl_2$ and undergoes charge reversal in $Ca(OH)_2$ at pH 11.8.

The compensation of the negative surface charge of C-S-H by the uptake of K^+ on C-S-H lowers significantly the alkali concentrations and thus the pH values in the surrounding solutions [44]. Lower pH values and alkali concentration are known to slow down or even prevent the formation of deleterious ASR products. Similarly the uptake of K^+ (and Na^+) by ASR products can lower the alkali concentrations and is thus expected to slow down the rate of ASR. Another important effect is the possible replacement of alkalis sorbed on the surface of C-S-H or ASR product by bivalent cations such as Ca^{2+}, which then releases the alkali back into the pore solution, where they re-participate in ASR over long time periods. The present study shows that C-S-H has a higher tendency to replace K^+ on its surface by Ca^{2+} than ASR product, such the alkali recycling will be more important for C-S-H than for ASR product. However, more significant than the replacement of surface bound K^+ or Na^+ by Ca^{2+} is the destabilisation of ASR product to C-S-H in the presence of high calcium concentrations as discussed in more detail in [5]. Such a destabilisation of ASR product will lead to the release of all alkalis bound and to higher KOH (and NaOH) concentrations in the solution, which can contribute again to the dissolution of aggregates and the formation of additional ASR products within the aggregates where little Ca is present.

The K^+ ions' affinity to ASR products indicates that such ASR products act as scavengers for alkalis and that their formation lowers the aqueous alkali concentrations and thus pH values in the pore solution and within the aggregate.

CRediT authorship contribution statement

N. Krattiger: Data acquisition and modelling, Formal analysis, Investigation, Writing – Original Draft, Visualization.

B. Lothenbach: Conceptualization, Methodology, Formal analysis, Validation, Writing – Review & Editing, Supervision.

S. Churakov: Conceptualization, Methodology, Validation, Data curation, Resources, Writing – Review & Editing, Supervision, Project administration.

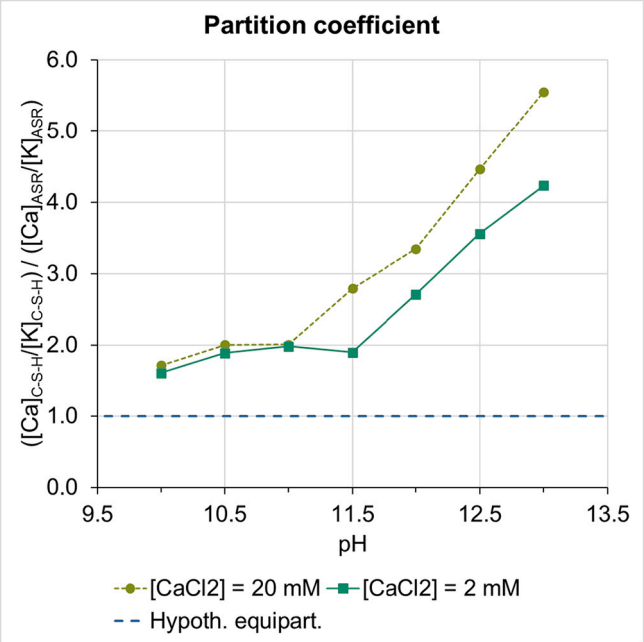

Fig. 7. Calculated Ca/K distribution coefficient (Eq. (4)) in the binary C-S-H/ASR system as function of pH.

Declaration of competing interest

The authors declare that they have no known competing financial interests or personal relationships that could have appeared to influence the work reported in this paper.

Acknowledgements

Zhenguo Shi is acknowledged for helpful discussions. Authors acknowledge access to the UBELIX HPC cluster at University of Bern. This research did not receive any specific grant from funding agencies in the public, commercial, or not-for-profit sectors.

Appendix A. Supplementary data

Supplementary data to this article can be found online at https://doi.org/10.1016/j.cemconres.2021.106491.

References

[1] R.N. Swamy, The Alkali-Silica Reaction in Concrete, CRC Press, London, 1991.
[2] M.A. Broekmans, B.J. Wigum, Alkali-aggregate Reaction in Concrete, Proceedings of the 13th International Conference on Alkali-Aggregate Reaction in Concrete, Trondheim, Norway, 2008.
[3] M. Ben Haha, E. Gallucci, A. Guidoum, K.L. Scrivener, Relation of expansion due to alkali silica reaction to the degree of reaction measured by SEM image analysis, Cem. Concr. Res. 37 (2007) 1206–1214.
[4] A. Leemann, Z. Shi, J. Lindgård, Characterization of amorphous and crystalline ASR products formed in concrete aggregates, Cem. Concr. Res. 137 (2020) 106190.
[5] Z. Shi, B. Lothenbach, The role of calcium on the formation of alkali-silica reaction products, Cem. Concr. Res. 126 (2019) 105898.
[6] A. Leemann, G. Le Saout, F. Winnefeld, D. Rentsch, B. Lothenbach, Alkali-silica reaction - the influence of calcium on silica dissolution and the formation of reaction products, J. Am. Ceram. Soc. 94 (2011) 1243–1249.
[7] Z. Shi, G. Geng, A. Leemann, B. Lothenbach, Synthesis, characterization, and water uptake property of alkali-silica reaction products, Cem. Concr. Res. 121 (2019) 58–71.
[8] Z. Shi, S. Park, B. Lothenbach, A. Leemann, Formation of shlykovite and ASR-P1 in concrete under accelerated alkali-silica reaction at 60 and 80 °C, Cem. Concr. Res. 137 (2020) 106213.
[9] I.V. Pekov, N.V. Zubkova, Y.E. Filinchuk, N.V. Chukanov, A.E. Zadov, D. Y. Pushcharovsky, E.R. Gobechiya, Shlykovite KCa[Si4O9(OH)] · 3H2O and cryptophyllite K2Ca[Si4O10] · 5H2O, new mineral species from the Khibiny

alkaline pluton, Kola Peninsula, Russia, in: Geology of Ore Deposits 52, 2010, pp. 767–777.
[10] G. Geng, Z. Shi, A. Leemann, C. Borca, T. Huthwelker, K. Glazyrin, I.V. Pekov, S. Churakov, B. Lothenbach, R. Dahn, E. Wieland, Atomistic structure of alkali-silica reaction products refined from X-ray diffraction and micro X-ray absorption data, Cem. Concr. Res. 129 (2020) 105958.
[11] Z. Shi, B. Lothenbach, The combined effect of potassium, sodium and calcium on the formation of alkali-silica reaction products, Cem. Concr. Res. 127 (2020) 105914.
[12] S.V. Churakov, Structure of the interlayer in normal 11 Å tobermorite from an ab initio study, Eur. J. Mineral. 21 (2009) 261–271.
[13] S.V. Churakov, Structural position of H_2O molecules and hydrogen bonding in anomalous 11 Å tobermorite, Am. Mineral. 94 (2009) 156–166.
[14] I.G. Richardson, Model structures for C-(A)-S-H(I), Acta Crystallogr. B70 (2014) 903–923.
[15] I.G. Richardson, The calcium silicate hydrates, Cem. Concr. Res. 38 (2008) 137–158.
[16] E. L'Hôpital, B. Lothenbach, K. Scrivener, D.A. Kulik, Alkali uptake in calcium alumina silicate hydrate (C-A-S-H), Cem. Concr. Res. 85 (2016) 122–136.
[17] B. Lothenbach, A. Nonat, Calcium silicate hydrates: solid and liquid phase composition, Cem. Concr. Res. 78 (2015) 57–70.
[18] S.V. Churakov, C. Labbez, Thermodynamics and molecular mechanism of Al incorporation in calcium silicate hydrates, J. Phys. Chem. C 121 (2017) 4412–4419.
[19] C. Labbez, I. Pochard, B. Jönsson, A. Nonat, C-S-H/solution interface: experimental and Monte Carlo studies, Cem. Concr. Res. 41 (2011) 161–168.
[20] S.V. Churakov, C. Labbez, L. Pegado, M. Sulpizi, Intrinsic acidity of surface sites in calcium-silicate-hydrates and its implication to their electrokinetic properties, J. Phys. Chem. C 118 (2014) 11752–11762.
[21] S.-Y. Hong, F.P. Glasser, Alkali binding in cement pastes: part I. The C-S-H phase, Cem. Concr. Res. 29 (1999) 1893–1903.
[22] C. Labbez, B. Jonsson, I. Pochard, A. Nonat, B. Cabane, Surface charge density and electrokinetic potential of highly charged minerals: experiments and Monte Carlo simulations on calcium silicate hydrate, J. Phys. Chem. B 110 (2006) 9219–9230.
[23] A. Vollpracht, B. Lothenbach, R. Snellings, J. Haufe, The pore solution of blended cements: a review, Mater. Struct. 49 (2016) 3341–3367.
[24] B. Lothenbach, F. Winnefeld, Thermodynamic modelling of the hydration of Portland cement, Cem. Concr. Res. 36 (2006) 209–226.
[25] J. Duchesne, M. Bérubé, The effectiveness of supplementary cementing materials in suppressing expansion due to ASR: another look at the reaction mechanisms part 2: pore solution chemistry, Cem. Concr. Res. 24 (1994) 221–230.
[26] M.H. Shehata, M.D. Thomas, R.F. Bleszynski, The effects of fly ash composition on the chemistry of pore solution in hydrated cement pastes, Cem. Concr. Res. 29 (1999) 1915–1920.
[27] M.H. Shehata, M.D.A. Thomas, Use of ternary blends containing silica fume and fly ash to suppress expansion due to alkali-silica reaction in concrete, Cem. Concr. Res. 32 (2002) 341–349.
[28] Z. Shi, C. Shi, S. Wan, Z. Zhang, Effects of alkali dosage and silicate modulus on alkali-silica reaction in alkali-activated slag mortars, Cem. Concr. Res. 111 (2018) 104–115.
[29] J. Lindgård, Ö. Andiç-Çakır, I. Fernandes, T.F. Rønning, M.D.A. Thomas, Alkali–silica reactions (ASR): literature review on parameters influencing laboratory performance testing, Cem. Concr. Res. 42 (2012) 223–243.
[30] F. Rajabipour, E. Giannini, C. Dunant, J.H. Ideker, M.D.A. Thomas, Alkali–silica reaction: current understanding of the reaction mechanisms and the knowledge gaps, Cem. Concr. Res. 76 (2015) 130–146.
[31] C. Labbez, B. Jönsson, M. Skarba, M. Borkovec, Ion−ion correlation and charge reversal at titrating solid interfaces, Langmuir 25 (2009) 7209–7213.
[32] N.V. Zubkova, Y.E. Filinchuk, I.V. Pekov, D.Y. Pushcharovsky, E.R. Gobechiya, Crystal structures of shlykovite and cryptophyllite: comparative crystal chemistry of phyllosilicate minerals of the mountainite family, Eur. J. Mineral. 22 (2010) 547–555.
[33] M. Lund, B. Jonsson, T. Pedersen, Activity coefficients in sea water using Monte Carlo simulations, Mar. Chem. 80 (2003) 95–101.
[34] C. Labbez, B. Joensson, A new Monte Carlo method for the titration of molecules and minerals, in: B. Kagstrom, E. Elmroth, J. Dongarra, J. Wasniewski (Eds.), Lecture Notes in Computer Science, Springer, 2007, pp. 66–72.
[35] G.M. Torrie, J.P. Valleau, Electrical double layers. I. Monte Carlo study of a uniformly charged surface, J. Chem. Phys. 73 (1980) 5807.
[36] D. Frenkel, B. Smit, Understanding Molecular Simulation, second ed., Academic Press, San Diego, 2002.
[37] Z. Abbas, E. Ahlberg, S. Nordholm, Monte Carlo simulations of salt solutions: exploring the validity of primitive models, J. Phys. Chem. B 113 (2009) 5905–5916.
[38] M. Pfeiffer-Laplaud, D. Costa, F. Tielens, M.-P. Gaigeot, M. Sulpizi, Bimodal acidity at the amorphous silica/water interface, J. Phys. Chem. C 119 (2015) 27354–27362.
[39] M. Pfeiffer-Laplaud, M.-P. Gaigeot, M. Sulpizi, pKa at quartz/electrolyte interfaces, J. Phys. Chem. Lett. 7 (2016) 3229–3234.
[40] S. Parashar, D. Lesnicki, M. Sulpizi, Increased acid dissociation at the quartz/water interface, J. Phys. Chem. Lett. 9 (2018) 2186–2189.
[41] M. Delhorme, C. Labbez, C. Caillet, F. Thomas, Acid−base properties of 2:1 clays. I. Modeling the role of electrostatics, Langmuir 26 (2010) 9240–9249.
[42] M. Porus, C. Labbez, P. Maroni, M. Borkovec, Adsorption of monovalent and divalent cations on planar water-silica interfaces studied by optical reflectivity and Monte Carlo simulations, J. Chem. Phys. 135 (2011), 064701.
[43] E. Bernard, Y. Yan, B. Lothenbach, Cation exchange capacity of calcium silicate hydrates (C-S-H), Cem. Concr. Res. 143 (2021), 106393.
[44] G. Plusquellec, A. Nonat, Interactions between calcium silicate hydrate (C-S-H) and calcium chloride, bromide and nitrate, Cem. Concr. Res. 90 (2016) 89–96.
[45] S. Barzgar, B. Lothenbach, M. Tarik, A. Di Giacomo, C. Ludwig, The effect of sodium hydroxide on Al uptake by calcium silicate hydrates (CSH), J. Colloid Interface Sci. 572 (2020) 246–256.